New Journal of Physics
The open access journal for physics

Josephson-coupled superconducting regions embedded at the interfaces of highly oriented pyrolytic graphite

A Ballestar, J Barzola-Quiquia, T Scheike and P Esquinazi[1]
Division of Superconductivity and Magnetism, Institut für Experimentelle Physik II, Universität Leipzig, Linnéstraße 5, D-04103 Leipzig, Germany
E-mail: esquin@physik.uni-leipzig.de

New Journal of Physics **15** (2013) 023024 (15pp)
Received 29 October 2012
Published 15 February 2013
Online at http://www.njp.org/
doi:10.1088/1367-2630/15/2/023024

Abstract. Transport properties of a few hundreds of nanometers thick (in the graphene plane direction) lamellae of highly oriented pyrolytic graphite (HOPG) have been investigated. Current–voltage characteristics as well as the temperature dependence of the voltage at different fixed input currents provide evidence for Josephson-coupled superconducting regions embedded in the internal two-dimensional interfaces of HOPG, reaching zero resistance at low enough temperatures.

Contents

[1] Author to whom any correspondence should be addressed.

1. Introduction

The existence of superconductivity in graphite-based compounds goes back to 1965 when it was first observed in potassium intercalated graphite C_8K [1]. Since then a considerable number of studies have reported this phenomenon, reaching critical temperatures $T_c \sim 10\,K$ in intercalated graphite [2, 3], above 30 K—although not percolative—in some highly oriented pyrolytic graphite (HOPG) samples [4] as well as in doped graphite [5–8]. Evidence for granular superconductivity in graphite powder at room temperature was obtained in the 1970s [9, 10]. Recent studies of the magnetic response of water-treated graphite powders [11] appear to confirm the existence of superconductivity at such high temperatures.

Theoretical works that deal with superconductivity in graphite as well as in graphene have been published in recent years. For example, p-type superconductivity has been predicted to occur in inhomogeneous regions of the graphite structure [12] or d-wave high-T_c superconductivity [13] based also on resonance valence bonds [14], or at the graphite surface region due to a topologically protected flat band [15]. Following a conventional Bardeen–Cooper–Schrieffer (BCS) approach in two dimensions (with anisotropy) a critical temperature $T_c \sim 60\,K$ has been estimated if the density of conduction electrons per graphene plane increases to $n \sim 10^{14}\,cm^{-2}$, a density that might be induced by defects and/or hydrogen ad-atoms [16] or by Li deposition [17]. Further predictions for superconductivity in graphene support the premise that $n > 10^{13}\,cm^{-2}$ in order to reach $T_c > 1\,K$ [18, 19]. The experimental work we describe in this paper deals with the existence of superconductivity at temperatures above 100 K in certain regions of ordered graphite samples.

Quite recently, this journal has published a new interpretation of the electrical resistance of HOPG samples [20], which is at odds with most of the published interpretation in the literature, in spite of the huge amount of experimental and theoretical research on the transport properties of graphite. The authors of [20] as well as of [21, 22] proposed that the earlier reported values of carrier density $n(T)$ and the metallic-like behavior of the resistivity $\rho(T)$ of highly oriented graphite samples, in general, are not intrinsic to an ideal, defect-free graphite with Bernal structure but are due, to a large extent, to the contribution of defective regions, in particular to two-dimensional internal interfaces running parallel to the graphene layers [21]. The nearly defect-free graphene layers inside the Bernal graphite matrix behave as a narrow gap semiconductor with an energy gap of the order of 40 meV [20].

Note that if we assume that the carrier density $n \gtrsim 10^{11}\,cm^{-2}$ obtained by different methods, such as Shubnikov–de Haas oscillations for example, in bulk graphite samples is concentrated mainly at the internal interfaces, the geometry normalized carrier density per graphene layer at the interfaces would then be several orders of magnitude larger. Therefore and within the theoretical predictions described above, one may expect that superconductivity could be localized at some of the internal interfaces found in highly oriented graphite samples [20, 21].

To fit the metallic-like behavior assumed to be due to the interfaces, a thermally activated exponential function was necessary [20]. It was suggested that this temperature dependence could be related to the existence of superconducting channels inside the interfaces in which thermal fluctuations can cause phase slips on the basis of the Langer–Ambegaokar–McCumber–Halperin model [23, 24] that applies to narrow superconducting channels. A series of different experimental hints obtained over the last few years indicate the possible existence of some kind of superconductivity in bulk graphite (see, e.g., [25–27]).

A direct proof of the existence of superconducting patches at some of the internal interfaces shown by transmission electron microscopy (TEM) studies [21] remains, however, open. Therefore, the main aim of the here presented experimental work is to measure the electrical response of a bundle of these internal interfaces found in HOPG samples, by contacting the voltage electrodes to several of them directly on their edges. The results of this work indicate that in these specially prepared lamellae some of the internal interfaces indeed show a granular superconducting behavior with clear evidence for Josephson-coupled superconducting regions. Upon sample and at low enough input current and temperature a zero resistance state is reached. To check the interpretation of the transport results, we have made magnetization measurements in a small bulk HOPG sample for magnetic fields normal to the interfaces. The observed behavior of the magnetization is compatible with granular superconductivity and supports the interpretation of the transport results.

This paper is organized as follows. In section 2, we explain how the specially made lamellae are prepared and contacted. From the experimental side and due to the difficulties involved, we believe that the sample preparation process and the measurement of the response of the internal interfaces is a major achievement of this work. In section 3, we show the voltage response of selected lamellae as a function of temperature at different input currents. These results indicate clearly that a transition occurs below a current-dependent temperature. In section 4, we present and discuss the results of current–voltage characteristic curves and the Josephson critical current obtained from them. Section 5 presents and discusses the effect of a magnetic field on the transport properties of the lamellae. Magnetization loops at a constant temperature and different maximum applied fields together with a short final discussion are given in section 6.

2. Sample characteristics

Thin TEM lamellae have been prepared from different HOPG bulk samples using a dual-beam microscope (FEI Nanolab XT200). To avoid contamination and structural disorder a 300 nm protective layer of tungsten carbide (WC) was deposited by Electron Beam Induced Deposition (EBID) on top of the HOPG surface. Previous studies on such WC layers prepared by EBID demonstrated that they are insulating [28] and therefore no contribution to the total measured resistance can be ascribed to this deposited material.

The Ga^+ ion beam was used to cut the lamellae of thickness between ~300 and 800 nm in the *a*–*b* graphene plane direction and lengths up to ~17 μm. The focused ion beam cutting process, upon the used fluence, induces a disordered graphite region with Ga implantation in the first 20 nm surface region of the lamellae (estimated using Monte-Carlo simulations given by the stopping range of ions in matter [29][2]). Energy dispersive x-ray spectroscopy (EDAX) measurements were made to check for the sample impurities revealing a concentration of ~2% of Ga in that surface near region. Independently done studies of the change in transport properties of thin graphite flakes after Ga^+ irradiation showed that the metallic-like behavior is destroyed and a large increase in electrical resistance is observed already at much lower Ga^+ fluences [30].

After transferring the lamellae to an insulating Si/SiN substrate, electron beam lithography followed by thermal evaporation of Pt/Au were used to make the four electrical contacts, allowing us to measure the voltage drop that occurs at several interfaces in parallel with the

[2] See also the simulation software IIS available at http://www.ele.uva.es/~jesman/iis.html, which has some advantages in comparison with the usual SRIM simulation.

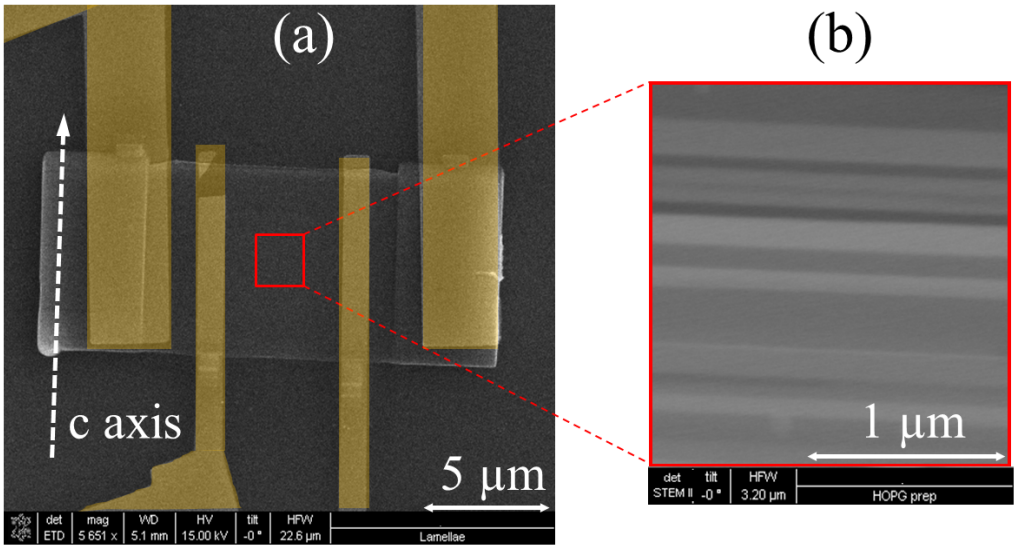

Figure 1. (a) Scanning electron microscopy image of sample L3 on an Si/SiN substrate where the yellow-colored areas are the electrodes. A four-point configuration has been prepared with the outer electrodes used to apply a current and the inner ones to measure the voltage drop. As shown in the picture, the *c*-axis runs parallel to the substrate surface and normal to the current direction. (b) TEM image of one HOPG lamella. Different brightnesses correspond to different orientations within the *a*–*b* plane of the crystalline regions of Bernal type.

graphene planes along a length of ∼2–8 μm. Four-probe electrode configuration as shown in figure 1(a) and also the van der Pauw configuration (contacts at lamella edges; see the inset in figure 4(b)) were used to measure the temperature dependence of voltage at constant input current and the *I*–*V* characteristic curves. The four-contact method used to measure the voltage response allows us to obtain the contribution of the inner part of the lamellae, i.e. of the non-modified region because its resistance with its interfaces is much smaller than the irradiated layer [30].

TEM studies on HOPG samples of high grade revealed single-crystalline regions of Bernal graphite of thickness between 30 nm and ∼200 nm in the *c*-axis direction [21]. Figure 1(b) shows a typical TEM image performed on one of the HOPG samples studied in this work. The different gray colors shown in figure 1(b) indicate sightly different angle misalignments about the *c*-axis between each other and the existence of very well defined two-dimensional interfaces between them. Rotations up to 30° between the graphene layers from neighboring graphite regions have been seen by high-resolution TEM in few-layer graphene sheets [31]. We note that the density of these interfaces (and probably also the defect and/or hydrogen concentration within the interfaces) depend on the HOPG batch and on the selected piece within a given batch. The total concentration of impurities measured by particle-induced x-ray emission is well below 15 ppm (see, e.g., [32]) and the rocking curve width of all the used HOPG samples (available from Advanced Ceramics or Momentive Performance Materials) is $0.4 \pm 0.1°$.

Although we found qualitatively similar results between the samples, the main difference in their transport properties depends on the used HOPG batch, on the selected region within

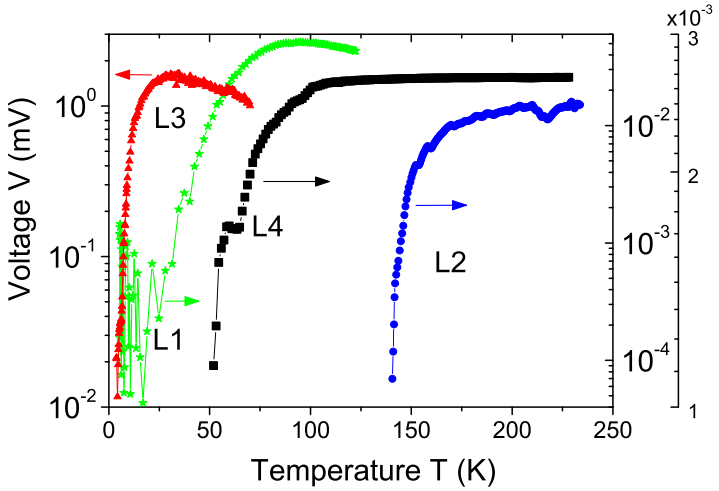

Figure 2. Temperature dependence of the voltage in a logarithmic scale for four samples measured with small input currents. A clear drop in the measured voltage is observed at 15 K $< T <$ 150 K upon sample. For the sample L4, the region near the onset of voltage decrease is shown (second right y-axis).

a selected batch and on the thickness used. Because the internal structure of bulk HOPG samples is not homogeneous in the micrometer range (see, e.g., [33][3]), i.e. different regions of the macroscopic sample can have different density of internal interfaces, the transport characteristics of the lamellae depend on the used piece. More than ten lamellae were studied coming from different batches. In this paper, we present and discuss the results of four of them (L1–L4) with thickness (∼500, ∼800, ∼300 and ∼800 nm), respectively. Samples L1, L3 and L4 were cut from the same batch and L2 from a different batch.

We note that there is no simple possibility to investigate locally a single interface with superconducting regions just because this is not simply accessible, at least with techniques such as scanning tunneling electron microscopy (STEM). First, one does not know which interface has superconducting regions and whether these patches would reach up to the interface edges. Therefore, we prepared samples with a large number of interfaces and contacted all of them in order to increase the probability to see the superconducting response in case it exists somewhere. Even if we would know in which of the interfaces superconducting regions exist, it is clear that we cannot simply open it and do STEM there because we would not have an interface anymore. After proving that superconductivity exists at some graphite interfaces, future experiments should try to localize them and other microscopic techniques are necessary to reveal their structural nature.

3. Temperature and input-current dependence of the measured voltage

Figure 2 shows the temperature dependence of the measured voltage at 1 nA (L1,L3) and 100 nA (L2,L4) input current. A clear drop in the measured voltage is observed, upon sample at different 'critical' temperatures T_c between ∼15 and ∼150 K. This T_c reflects the temperature above which the Josephson coupling between superconducting patches at some of the interfaces

[3] See also the comment by Sadewasser and Glatzel, and the replies by Lu *et al* and also Proksch [33].

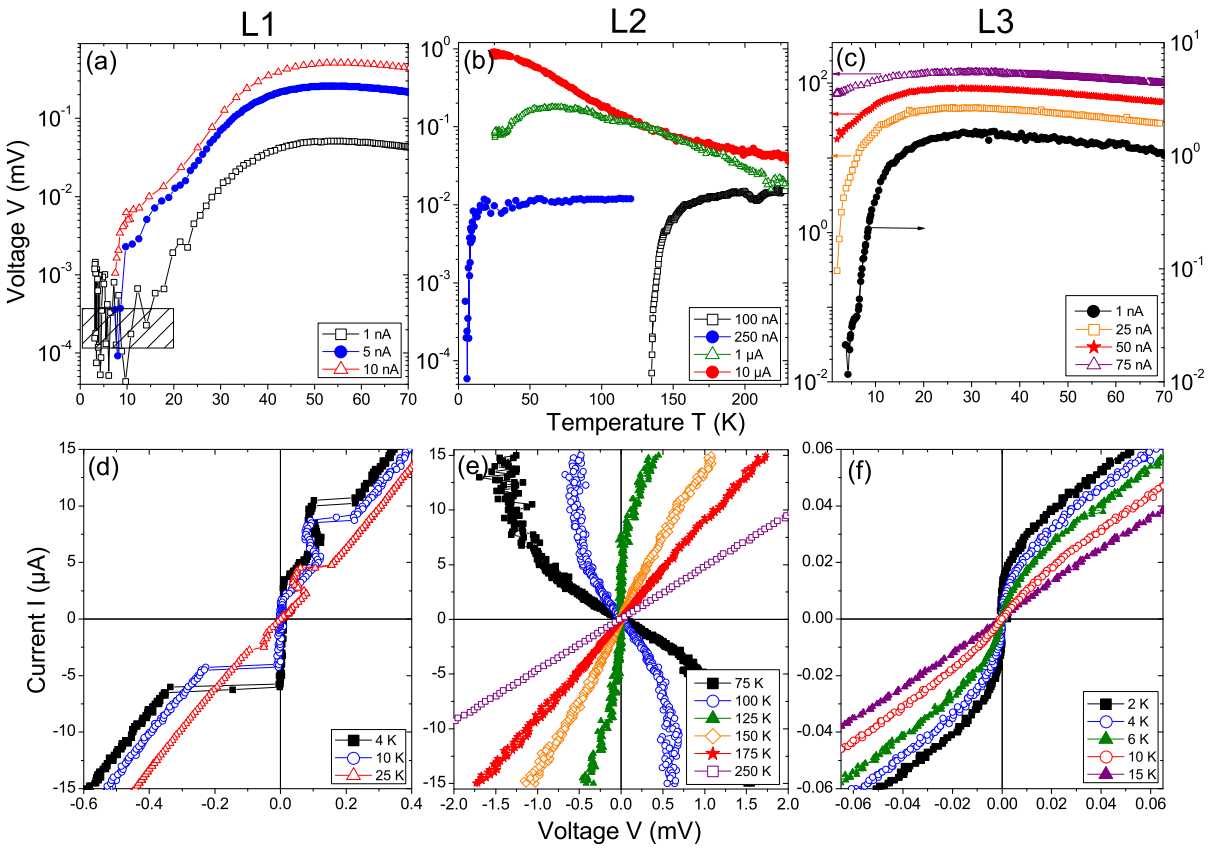

Figure 3. (a)–(c) Voltage versus temperature at different input currents for samples L1–L3. The shady region in (a) depicts the 300 nV noise region of sample L1 at low temperatures. This noise is intrinsic to the sample and vanishes after the application of a magnetic field (see figure 6(a) inset). (d)–(f) The I–V characteristic curves at different temperatures for the same samples.

vanishes. At low enough temperatures and currents zero resistance states were reached for L1, L3 and L4. A negative saturation voltage, instead of zero, is obtained for sample L2 because of the van der Pauw configuration used, which can be quantitatively explained using a simple Wheatstone bridge circuit as explained in section 4.

The observed T-dependence in figure 2, in particular the clear drop below a certain temperature, is determined by the internal interfaces, since the graphene layers within the crystalline regions show a semiconducting narrow-band-gap behavior [20]. Lamellae as well as bulk HOPG samples with a much lower density of interfaces show a semiconducting behavior as well as no Shubnikov–de Haas or de Haas–van Alphen oscillations in the magnetoresistance or magnetization [34].

If the voltage drop is related to some kind of granular superconductivity we expect that its temperature dependence is sensitively influenced by the applied current. Figures 3(a)–(c) clearly show that the higher the input current the lower the transition temperature, revealing a semiconducting-like behavior at higher I and T. The observed behavior is compatible with the existence of granular superconductivity (see, e.g., [35]) embedded in some of the internal interfaces. We emphasize that for samples without internal interfaces only a semiconducting behavior with saturation at low temperatures is measured [21]. The saturation of the voltage at

low temperatures, see, e.g., figure 3(b), is due to the parallel contribution of the surfaces of the sample that prevent an infinite enhancement of the resistance [20]. We would like to remark here that a further proof that we are indeed measuring graphite is the fact that for high input currents, where the Josephson coupling effectively vanishes, see figure 3(b), we measure the usual temperature behavior known for graphite thin films without interfaces [20, 21].

4. Current–voltage characteristics

Further support of the claim that we have a granular superconductivity behavior due to the internal interfaces is obtained from the I–V characteristic curves. Samples L1 (figure 3(d)) and L3 (figure 3(f)) show a typical Josephson behavior and a zero resistance state is clearly observed. In the case of sample L1, a sharp jump in the current appears at the corresponding critical Josephson current I_c, where also a small hysteresis is observed, see figure 3(d). Therefore, in that sample we have a junction with a large capacitance (underdamped limit).

In the case of sample L3, the obtained characteristic I–V curves can be understood with the model proposed by Ambegaokar and Halperin [36] (see also [37]). Their model is based on a Josephson junction with a small capacitance (overdamped limit) where the thermal fluctuations disrupt the coupling of the phases of the two superconductors, resulting in a noise voltage with a non-zero average value. They use an analogy with the Brownian motion of a particle in a field of force giving the following equation:

$$\upsilon \equiv \frac{V}{I_c R} = \frac{4\pi}{\gamma}\left\{(e^{\pi\gamma x}-1)^{-1}\int_0^{2\pi} d\theta f(\theta)\int_0^{2\pi} d\theta' \frac{1}{f(\theta')} + \int_0^{2\pi} d\theta \int_\theta^{2\pi} d\theta' \frac{f(\theta)}{f(\theta')}\right\}^{-1}, \qquad (1)$$

where υ is the potential difference in reduced units; V is the mean experimentally measured voltage; I_c is the critical Josephson current at a certain temperature T; R is the resistance of the junction (for $T \simeq T_c$ (transition temperature) it may be approximated by the resistance in the normal state); γ is defined as $\gamma = \frac{I_c \hbar}{ekT}$ and x as $x = \frac{I}{I_c}$ (current in reduced units); and $f(\theta) = e^{\gamma(x\theta+\cos\theta)/2}$, where θ is the difference in the phases of the order parameter on opposite sides of the junction. Figure 4(a) shows the experimental I–V characteristic curves in reduced units for sample L3 at different temperatures. With the model described above and having I_c as the only free parameter, we obtain the results presented by the solid lines in that figure. The theoretical model fits the experimental data very well.

In the case of sample L2 (figure 3(e)) the curves were obtained with a van der Pauw configuration and current and voltage paths that may get the answer of more than one Josephson junction in that sample, for a current–voltage electrode configuration as seen in the inset of figure 4(b). To understand quantitatively the observed behavior we use a simple Wheatstone bridge circuit, see the inset of figure 4(b), where the measured voltage difference for a given current is given by the contribution of effective resistances R_i following the equation

$$V \propto \frac{R_1 R_4 - R_2 R_3}{(R_1+R_2)(R_3+R_4)}. \qquad (2)$$

If one assumes that $R_1(I)$ is a resistance influenced by a single pair of Josephson-coupled superconducting grains in that path, we may use equation (1) to describe the behavior of $R_1(I)$. For this case, we obtain $V < 0$ if $R_1 = 0$ and the input current $0 < I < I_c(T)$, where I_c is the corresponding effective Josephson critical current of the junction. If we consider now that R_2 is

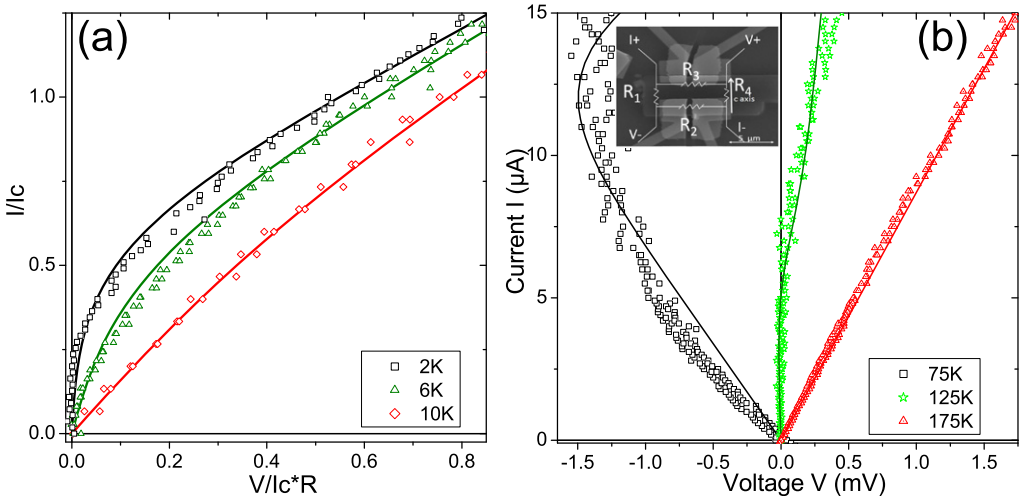

Figure 4. Current–voltage characteristics at different temperatures for samples L3 (a) and L2 (b), the first one in reduced coordinates where R is the normal state resistance. The continuous curves are fits to the model proposed in [36] with the Josephson critical current $I_c(T)$ as the only free parameter. The inset in (b) shows a scanning electron microscope image of the L2 sample with the van der Pauw configuration of the electrodes and one possible selection of current and voltage electrodes, which corresponds to the experimental data for sample L2 in the main panel.

also influenced by Josephson-coupled superconducting grains, then $V \approx 0$, < 0 or > 0 can be achieved depending on the relative values of R_1 and R_2. Furthermore, if the other resistances R_i follow the Josephson behavior, a noisy voltage around zero will be measured. The solid lines in figure 4(b) correspond to the calculated voltage applying this model for sample L2. The model explains reasonably well the experimental data assuming two resistors that follow the Josephson behavior (equation (1)) but with two different critical currents. Selecting different current and voltage electrodes within the same van der Pauw configuration we obtain different I–V curves, all of them can be well understood with the above equations selecting different critical Josephson currents.

Considering the I–V results from all samples and configurations we obtain $I_c(T)$ shown in figure 5 in normalized units. The overall behavior is compatible with the temperature dependence expected for Josephson junctions where the normal barrier is given by ballistic graphene [38], the solid line in figure 5. One may ask whether a Josephson coupling is possible through graphene layers and at large distances. Indeed, the work in [39] showed experimentally that the Josephson effect is possible between superconducting electrodes separated by a hundreds of nanometers long graphene path. Therefore, the assumption of existence of Josephson-coupled superconducting regions through graphene-like semiconducting paths at the observed interfaces appears reasonable. Because these superconducting regions at the interfaces are not homogeneously distributed in the samples used, upon the junctions distribution, a noisy or 'jumpy' behavior of the voltage is expected at low enough temperatures and currents due to phase and current path fluctuations. We have observed this behavior in samples L1, see the figure 3(a), and L2, see the inset in figure 6(a). This noisy behavior is

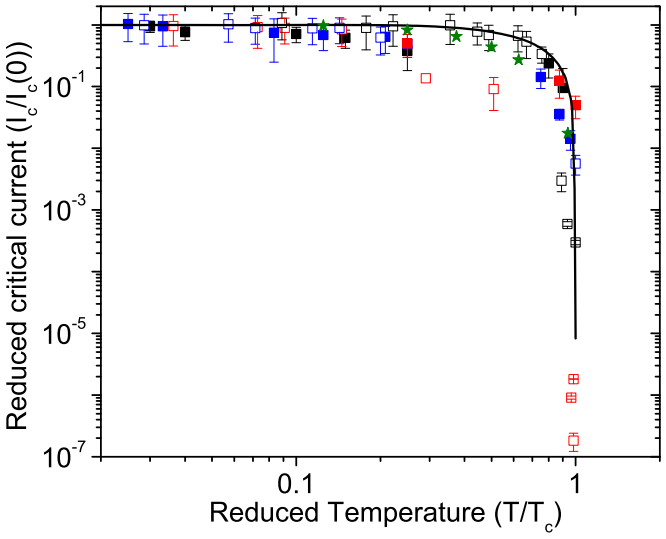

Figure 5. Normalized Josephson critical current $I_c/I_c(0)$ versus normalized T/T_c obtained for different lamellae (each symbol corresponds to a different samples and/or configurations in the measurements). Critical currents between 55 nA and 5.5 μA and critical temperatures from 15 K up to 175 K have been used. The continuous line is the theoretical curve taken from [38] without any free parameter, assuming a short junction length.

intrinsic to the samples and can be suppressed by applying a magnetic field normal to the graphene planes, see the inset in figure 6(a). Future work should reveal the frequency spectrum of the noise and its relation to the Josephson junction arrangement in the samples.

5. The influence of a magnetic field

An applied magnetic field is expected to be detrimental to the superconducting state. This effect can be due to an orbital depairing effect, i.e. a critical increase of the shielding currents, or at much higher fields due to the alignment of the electron spins, in the case of singlet coupling. However, the possible effects of a magnetic field on the superconducting state of quasi-two-dimensional superconductors or in case the coupling does not correspond to a singlet state are not that clear. For example, recently published experimental results [40] in two different two-dimensional superconductors, including the one produced at the interfaces between nonsuperconducting regions, show that superconductivity can be even enhanced by a parallel magnetic field. In case the pairing is p-type [12], the influence of a magnetic field is expected to be qualitatively different from the conventional behavior [41, 42] with even an enhancement of the superconducting state at intermediate fields in case the orbital diamagnetism can be neglected or for parallel field configuration. On the other hand, even for applied fields normal to the planes, we expect much less influence of the orbital effect in case the London penetration depth is much larger than the size of the superconducting regions at the interfaces of our lamellae. If the superconducting coherence length is of the order of or larger than the thickness of the lamella, then we expect a superconducting (granular) behavior at lower T but a magnetic field may be much less detrimental.

We have studied the effects of magnetic fields applied parallel and normal to the interfaces on the transport characteristics in all measured lamellae. Upon sample the observed effects of an applied magnetic field are from no effect at all, the usual vanishing of the zero resistance state at relatively low fields applied normal to the interfaces to a partial recovery of the superconducting state at high enough applied fields. It should be clear that any measurable effect of a magnetic field on the measured transport signals of our lamellae does not provide necessarily the critical fields of the superconducting regions, but mainly its influence on the coupling between them. Therefore, the somehow usual measurement of the upper critical field $H_{c2}(T)$ appears to be at this stage of our research not possible.

Figure 6 shows the I–V characteristics of samples L4 (a) and L3 (b). For the relatively thick lamella L4 a magnetic field of 1 T applied normal to the interface planes vanishes the zero resistance state observed at zero field and at 50 K. At higher fields, however, the I–V curves show a recovery to the zero resistance state. We emphasize that in this case a field applied parallel to the interface planes does not affect the curves at all up to 8 T, within experimental error. Recent studies on possible superconductivity triggered by a large enough electric field applied on multigraphene samples revealed also a kind of reentrance above a certain magnetic field applied normal to the graphene layers [43]. For the thinnest sample L3, however, a magnetic field applied in both directions has little or no effect on the I–V characteristics or $V(T)$ up to 8 T, see figure 6(b) and its inset.

6. Discussion and conclusion

Certainly, further support to our interpretation can be provided by magnetization measurements of the lamellae. However, the sample mass of these tiny lamellae is far too small to be measurable with a commercial superconducting quantum interferometer device (SQUID). Nevertheless, we have prepared a HOPG sample of size 1 mm × 4 mm × 0.2 mm from the same batch of sample L2 and measured the hysteresis loops with the field applied normal to the graphene planes. As an example, we show the results at 100 K in figure 7. The observed changes of the hysteresis as a function of the maximum applied field, namely from a reversible (zero hysteresis) at low maximum applied fields ($H \lesssim 100$ Oe) to a Bean-like behavior at fields of the order of 300 Oe, to the narrowing of the hysteresis at the largest fields, agrees with that expected for granular superconductors [44–46], as has recently been reported for water-treated graphite powders [11]. The change in the slope of the virgin first curve is also typical of a granular superconducting response.

It is interesting to note that no hysteresis was observed for fields applied parallel to the interfaces. Furthermore, one can find HOPG samples where no hysteresis of any kind can be measured, in spite of a similar diamagnetic response. This result rules out the influence of SQUID artifacts in the presented loops. Clearly, the larger the sample area and thickness, the larger the probability to get interfaces with higher critical temperatures inside the sample. Therefore, in principle, it appears possible that the granular superconducting behavior is seen at higher temperatures in the magnetization of larger samples than in the transport properties of tiny lamellae.

The possibility of high-temperature superconductivity at surfaces and interfaces has attracted the attention of the low-temperature physics community since the 1960s [47]. Recently, superconductivity was found at the interfaces between oxide insulators [48] as well as between metallic and insulating copper oxides with $T_c \gtrsim 50$ K [49]. In the case of doped

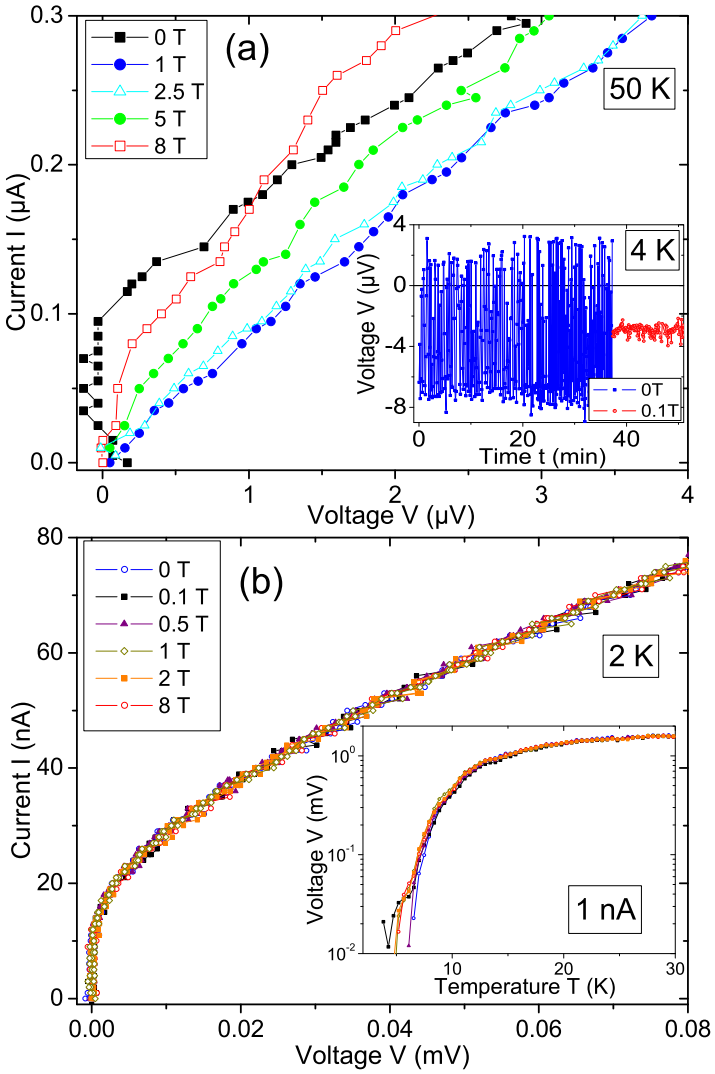

Figure 6. (a) Current–voltage curves for sample L4 at 50 K with and without magnetic field perpendicular to the graphene planes up to 8 T. The inset shows the time dependence of the voltage in sample L2 for 250 nA input current at a constant temperature of 4 K, with no applied magnetic field (blue squares) and at 0.1T field applied perpendicular to the graphene planes (red dots). (b) Current–voltage characteristic curves for sample L3 at 2 K with magnetic field applied parallel to the graphene planes up to 8 T. The inset shows the temperature dependence of the voltage with 1 nA input current for sample L3 for magnetic fields from zero (blue circles) up to 8 T (red dots) applied normal to the graphene planes.

semiconductors the example of Bi is of interest; interfaces in Bi bicrystals of inclination type show superconductivity up to 21 K, although Bi bulk is not a superconductor [50]. We think that these two independently obtained indications and the special role of interfaces shown here should stimulate further characterization and studies to generate highly doped regions in graphite at specially produced interfaces.

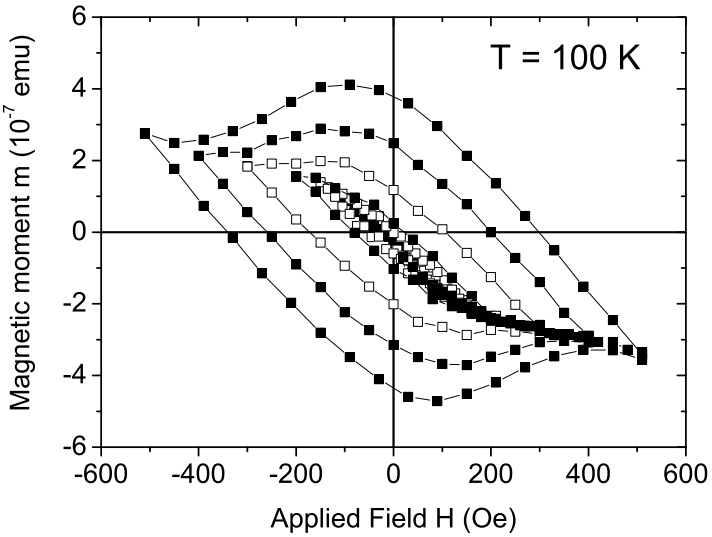

Figure 7. Magnetic moment as a function of field applied normal to the graphene planes and the interfaces of a HOPG sample of mass $m = 1.4$ mg at 100 K. A constant diamagnetic slope was subtracted from the measured data. Each hysteresis has been obtained for a given maximum applied magnetic field.

The existence of domains of rhombohedral stacking have recently been identified in exfoliated few-layer graphene samples [51]. Also rhombohedral crystallites embedded in the usual Bernal-type graphite blocks were identified by high-resolution TEM [52]. A recent theoretical work in [53] suggests the existence of very high temperature surface superconductivity in rhombohedral graphite with very high anisotropy. The theoretical results indicate that this superconductivity is basically two dimensional, providing an explanation for the huge anisotropy observed in the SQUID and transport measurements of large enough samples. We may speculate, therefore, that part of the observed interfaces in our HOPG lamellae contains this kind of stacking order with high superconducting critical temperatures.

Finally, we would like to renew a rather forgotten discussion on the interpretation of the huge magnetic field-driven, metal–insulator transition (MIT) observed in the longitudinal resistance of bulk graphite samples [54–58]. The interpretation given in [57, 58] was based on an intrinsic property of graphite related to transport parameters used in the two-band or three-band model. This interpretation is clearly at odds with the one given in [54], which suggested a superconducting origin. We believe that our results finally clarify that the origin of the metallic-like behavior as well as the giant magnetic-field-induced MIT measured in HOPG in the past is related, to a large extent, to the superconducting properties of internal interfaces and it is not intrinsic of the graphite structure. The fact that the metallic-like behavior observed in thick enough graphite samples vanishes for thinner ones [20, 21, 59] does not support the assumed intrinsic origin of the MIT. We further note that the reentrance to a metallic-like state at low temperatures observed in the longitudinal resistance at high enough magnetic fields [56] might be related to the magnetic-field-driven reentrance observed in our lamellae, see figure 6(a), as well as in the electric field-induced transition [43]. In conclusion, the transport characteristics of thin lamellae with tens of two-dimensional interfaces between crystalline graphite regions reveal a Josephson-like behavior with zero resistance states at low enough temperatures and input currents.

Acknowledgments

This work was supported by the Deutsche Forschungsgemeinschaft under contract no. DFG ES 86/16-1. AB was supported by ESF-Nano under the Graduate School of Natural Sciences 'BuildMona'.

References

[1] Hannay N B, Geballe T H, Matthias B T, Andres K, Schmidt P and Mac Nair D 1965 Superconductivity in graphitic compounds *Phys. Rev. Lett.* **14** 225–6
[2] Weller T E, Ellerby M, Siddharth S S, Smith R P and Skippe T 2005 Superconductivity in the intercaled graphite compounds C_6Yb and C_6Ca *Nature Phys.* **1** 39–41
[3] Emery N, Hérold C, D'Astuto M, Garcia V, Bellin Ch, Marêché J F, Lagrange P and Loupias G 2005 Superconductivity of bulk CaC_6 *Phys. Rev. Lett.* **95** 035413
[4] Kopelevich Y, Esquinazi P, Torres J H S and Moehlecke S 2000 Ferromagnetic- and superconducting-like behavior of graphite *J. Low Temp. Phys.* **119** 691–702
[5] Ricardo da Silva R, Torres J H S and Kopelevich Y 2001 Indication of superconductivity at 35 K in graphite–sulfur composites *Phys. Rev. Lett.* **87** 147001–1–4
[6] Kopelevich Y, da Silva R R, Torres J H S, Moehlecke S and Maple M B 2004 High-temperature local superconductivity in graphite–sulfur composites *Physica* C **408** 77–8
[7] Felner I and Kopelevich Y 2009 Magnetization measurement of a possible high-temperature superconducting state in amorphous carbon doped with sulfur *Phys. Rev.* B **79** 233409
[8] Kopelevich Y and Esquinazi P 2007 Ferromagnetism and superconductivity in carbon-based systems *J. Low Temp. Phys.* **146** 629–39
[9] Antonowicz K 1974 Possible superconductivity at room temperature *Nature* **247** 358–60
[10] Antonowicz K 1975 The effect of microwaves on dc current in an Al–carbon–Al sandwich *Phys. Status Solidi* a **28** 497–502
[11] Scheike T, Böhlmann W, Esquinazi P, Barzola-Quiquia J, Ballestar A and Setzer A 2012 Can doping graphite trigger room temperature superconductivity? Evidence for granular high-temperature superconductivity in water-treated graphite powder *Adv. Mater.* **24** 5826–31
[12] González J, Guinea F and Vozmediano M A H 2001 Electron–electron interactions in graphene sheets *Phys. Rev.* B **63** 134421–1–8
[13] Nandkishore R, Levitov L S and Chubukov A V 2012 Chiral superconductivity from repulsive interactions in doped graphene *Nature Phys.* **8** 158–63
[14] Black-Schaffer A M and Doniach S 2007 Resonating valence bonds and mean-field d-wave superconductivity in graphite *Phys. Rev.* B **75** 134512
[15] Kopnin N B, Heikkilä T T and Volovik G E 2011 High-temperature surface superconductivity in topological flat-band systems *Phys. Rev.* B **83** 220503
[16] García N and Esquinazi P 2009 Mean field superconductivity approach in two dimensions *J. Supercond. Nov. Magn.* **22** 439–44
[17] Profeta G, Calandra M and Mauri F 2012 Phonon-mediated superconductivity in graphene by lithium deposition *Nature Phys.* **8** 131–4
[18] Bruno Uchoa and Castro A H Neto 2007 Superconducting states of pure and doped graphene *Phys. Rev. Lett.* **98** 146801
[19] Kopnin N B and Sonin E B 2008 BCS superconductivity of Dirac electrons in graphene layers *Phys. Rev. Lett.* **100** 246808
[20] García N, Esquinazi P, Barzola-Quiquia J and Dusari S 2012 Evidence for semiconducting behavior with a narrow band gap of `Bernal` graphite *New J. Phys.* **14** 053015

[21] Barzola-Quiquia J, Yao J-L, Rödiger P, Schindler K and Esquinazi P 2008 Sample size effects on the transport properties of mesoscopic graphite samples *Phys. Status Solidi* a **205** 2924–33
[22] Arndt A, Spoddig D, Esquinazi P, Barzola-Quiquia J, Dusari S and Butz T 2009 Electric carrier concentration in graphite: dependence of electrical resistivity and magnetoresistance on defect concentration *Phys. Rev.* B **80** 195402
[23] Langer J S and Ambegaokar V 1967 Intrinsic resistive transition in narrow superconducting channels *Phys. Rev.* **164** 498–510
[24] McCumber D E and Halperin B I 1970 Time scale of intrinsic resistive fluctuations in thin superconducting wires *Phys. Rev.* B **1** 1054–70
[25] Esquinazi P, García N, Barzola-Quiquia J, Rödiger P, Schindler K, Yao J-L and Ziese M 2008 Indications for intrinsic superconductivity in highly oriented pyrolytic graphite *Phys. Rev.* B **78** 134516
[26] Dusari S, Barzola-Quiquia J and Esquinazi P 2011 Superconducting behavior of interfaces in graphite: transport measurements of micro-constrictions *J. Supercond. Nov. Magn.* **24** 401–5
[27] Barzola-Quiquia J and Esquinazi P 2010 Ferromagnetic- and superconducting-like behavior of the electrical resistance of an inhomogeneous graphite flake *J. Supercond. Nov. Magn.* **23** 451–5
[28] Spoddig D, Schindler K, Rödiger P, Barzola-Quiquia J, Fritsch K, Mulders H and Esquinazi P 2007 Transport properties and growth parameters of PdC and WC nanowires prepared in a dual-beam microscope *Nanotechnology* **18** 495202
[29] Ziegler J F, Biersack J P and Ziegler M D 2008 *SRIM— The Stopping and Range of Ions in Matter* ISBN:0-9654207-1-X
[30] Barzola-Quiquia J, Dusari S, Bridoux G, Bern F, Molle A and Esquinazi P 2010 The influence of Ga^+ irradiation on the transport properties of mesoscopic conducting thin films *Nanotechnology* **21** 145306
[31] Warner J H, Römmeli M H, Gemming T, Büchner B and Briggs G A D 2009 Direct imaging of rotational stacking faults in few layer graphene *Nano Lett.* **9** 102–6
[32] Ohldag H, Esquinazi P, Arenholz E, Spemann D, Rothermel M, Setzer A and Butz T 2010 The role of hydrogen in room-temperature ferromagnetism at graphite surfaces *New J. Phys.* **12** 123012
[33] Lu Y, Muñoz M, Steplecaru C S, Hao C, Bai M, García N, Schindler K and Esquinazi P 2006 Electrostatic force microscopy on oriented graphite surfaces: coexistence of insulating and conducting behaviors *Phys. Rev. Lett.* **97** 076805
Sadewasser S and Glatzel Th 2007 *Phys. Rev. Lett.* **98** 269701
Lu *et al* 2007 *Phys. Rev. Lett.* **98** 269702
Proksch R 2006 *Appl. Phys. Lett.* **89** 113121
[34] Camargo B C, Kopelevich Y, Hubbard S B, Usher A, Böhlmann W and Esquinazi P 2012 Effect of structural disorder on the quantum oscillations in graphite, in preparation
[35] Berdnorz J G and Müller K A 1986 *Z. Phys.* B **64** 189
[36] Ambegaokar V and Halperin B I 1969 Voltage due to thermal noise in the dc Josephson effect *Phys. Rev. Lett.* **22** 1364–6
[37] Ivanchenko Yu M and Zil'berman L A 1968 The Josephson effect in small tunnel contacts *Zh. Eksp. Teor. Fiz.* **55** 2395–402
Ivanchenko Yu M and Zil'berman L A 1969 *Sov. Phys.—JETP* **28** 1272–6
Ivanchenko Yu M and Zil'berman L A 1968 *Zh. Eksp. Teor. Fiz. Pis. Red.* **8** 189–92
Ivanchenko Yu M and Zil'berman L A 1968 *JETP Lett.* **8** 113–5
[38] Hagymási I, Kormányos A and Cserti J 2010 Josephson current in ballistic superconductor-graphene systems *Phys. Rev.* B **82** 134516
[39] Heersche H B, Jarillo-Herrero P, Oostinga J B, Vandersypen L M K and Morpurgo A F 2007 Bipolar supercurrent in graphene *Nature* **446** 56–9
[40] Gardner H J, Kumar A, Yu L, Xiong P, Warusawithana M P, Wang L, Vafek O and Schlom D G 2011 Enhancement of superconductivity by a parallel magnetic field in two-dimensional superconductors *Nature Phys.* **7** 895–900

[41] Scharnberg K and Klemm R A 1980 p-wave superconductors in magnetic fields *Phys. Rev.* B **22** 5233–44
[42] Knigavko A and Rosenstein B 1998 Spontaneous vortex state and ferromagnetic behavior of type-II p-wave superconductors *Phys. Rev.* B **58** 9354–64
[43] Ballestar A, Barzola-Quiquia J, Dusari S, Esquinazi P, da Silva R R and Kopelevich Y 2012 Electric field induced superconductivity in multigraphene arXiv:1202.3327
[44] Senoussi S, Aguillon C and Hadjoudj S 1991 The contribution of the intergrain currents to the low field hysteresis cycle of granular superconductors and the connection with the micro- and macrostructures *Physica* C **175** 215–25
[45] Borik M, Chernikov M, Veselago V and Stepankin V 1991 Anomalies of the magnetic properties of granular oxide superconductor $BaPb_{l-x}Bi_xO_3$ *J. Low Temp. Phys.* **85** 283–94
[46] Andrzejewski B, Guilmeau E and Ch. Simon 2001 Modelling of the magnetic behaviour of random granular superconductors by the single junction model *Supercond. Sci. Technol.* **14** 904–9
[47] Ginzburg V L 1964 On surface superconductivity *Phys. Lett.* **13** 101–2
[48] Reyren N *et al* 2007 Superconducting interfaces between insulating oxides *Science* **317** 1196–9
[49] Gozar A, Logvenov G, Fitting Kourkoutis L, Bollinger A T, Giannuzzi L A, Muller L A and Bozovic I 2008 High-temperature interface superconductivity between metallic and insulating copper oxides *Nature* **455** 782–5
[50] Muntyanua F M, Gilewski A, Nenkov K, Zaleski A and Chistol V 2008 Superconducting crystallite interfaces with T_c up to 21 K in Bi and Bi–Sb bicrystals of inclination type *Solid State Commun.* **147** 183
[51] Lui C H, Li Z, Chen Z, Klimov P V, Brus L E and Heinz T F 2011 Imaging stacking order in few-layer graphene *Nano Lett.* **11** 164–9
[52] Lin Q, Li T, Liu Z, Song Y, He L, Hu Z, Guo Q and Ye H 2012 High-resolution TEM observations of isolated rhombohedral crystallites in graphite blocks *Carbon* **50** 2369–71
[53] Kopnin N B and Heikkila T T 2012 Surface superconductivity in rhombohedral graphite arXiv:1210.7075
[54] Kempa H, Kopelevich Y, Mrowka F, Setzer A, Torres J H S, Höhne R and Esquinazi P 2000 Magnetic field driven superconductor–insulator-type transition in graphite *Solid State Commun.* **115** 539–42
[55] Kempa H, Esquinazi P and Kopelevich Y 2002 Field-induced metal–insulator transition in the *c*-axis resistivity of graphite *Phys. Rev.* B **65** 241101
[56] Kopelevich Y, Torres J H S, da Silva R R, Mrowka F, Kempa H and Esquinazi P 2003 Reentrant metallic behavior of graphite in the quantum limit *Phys. Rev. Lett.* **90** 156402–1–4
[57] Tokumoto T, Jobiliong E, Choi E S, Oshima Y and Brooks J S 2004 Electric and thermoelectric transport probes of metal–insulator and two-band magnetotransport behavior in graphite *Solid State Commun.* **129** 599
[58] Du X, Tsai S-W, Maslov D L and Hebard A F 2005 Metal–insulator-like behavior in semimetallic bismuth and graphite *Phys. Rev. Lett.* **94** 166601
[59] Ohashi Y, Yamamoto K and Kubo T 2001 Shubnikov de–Haas effect of very thin graphite crystals *Carbon'01: An Int. Conf. on Carbon* (*Lexington, 14–19 July*)